

Image Segmentation of Secondary Septa in Lungs

H.-S. Wu, L. Deligdisch and M. I. Fiel

Department of Pathology, Mount Sinai School of Medicine, Box 1194, One Gustave L. Levy Place, New York,
New York 10029

E-mail: haishan.wu@mssm.edu

T. Schiano

Division of Liver Diseases, The Mount Sinai Medical Center, Box 1104, One Gustave Levy Place, New York,
New York 10029

J. Gil

Department of Pathology, Mount Sinai School of Medicine, Box 1194, One Gustave L. Levy Place, New York,
New York 10029

Abstract. An algorithm for image segmentation of the secondary septa in the lungs using light microscopy is presented. After converting the original analog image to binary with proper thresholding, morphological operations are applied to individual lumen regions to extract the secondary septum regions that appear as cavelike regions in each lumen. To reduce the errors of misclassifying the primary septa from secondary septa because of the occasional leaks in the broken primary septum lines, a gap-closing procedure is designed before another separation procedure of the secondary septa is executed. The algorithm is applied to real lung images of both normal and cancerous lungs. The results show that the algorithm is robust and is able to identify and segment the secondary septa in lungs effectively. © 2011 Society for Imaging Science and Technology.

[DOI: 10.2352/J.ImagingSci.Technol.2011.55.1.010508]

INTRODUCTION

The human lung is largely of a saccular conformation containing mainly smooth-walled channels and terminal sacculi at birth.¹ The channels later transform into alveolar ducts and the sacculi into alveolar sacs via the outgrowth of new secondary septa from the saccular walls of the primary septa.^{1,2} After their development in infancy, the human lungs increase in size but not complexity.³ In a study of the normal and hypoplastic lungs at the pseudoglandular stage, Chinoy et al.⁴ showed that after implantation of the lungs, larger airspaces and formation of secondary septa appear in normal lungs, whereas hypoplastic lungs have defective saccular structures and no secondary septa.

Tschanz and Burri⁵ previously proposed an algorithm measuring the septum length by counting the number of points in each segment of one-pixel-wide lines skeletonized from binary images. McCurnin et al.⁶ used this skeleton algorithm to study the morphologic effects of the persistent patent ductus arteriosus in a preterm baboon model of

bronchopulmonary dysplasia. Hosgör et al.⁷ showed the thickening effects of alveolar walls from the fibrin deposition in lung septal capillaries. Boucherat et al.⁸ observed that congenital diaphragmatic hernia (CDH) occurring in human lungs presents thicker alveolar septa. They also found that, in control fetuses, lung parenchyma matured homogeneously during the period with thinning of septal walls and a surge of secondary septa while CDH lungs displayed thicker walls and deficiency in secondary septa.⁸ Foster et al.⁹ hypothesized that the tips of secondary alveolar septa contain differentially expressed gene products and showed that several gene products, including galectin-1, are enriched in the tips of these alveolar secondary septa.

While visual observation may reveal subjective estimation of septa, the quantitative analysis of septa requires segmentation of septum regions from the images. There are numerous algorithms designed for segmentation of medical images.^{10–16} However, very little has been done with the segmentation of lung septa. While a primary septum connects other septa on both its ends, a secondary septum outgrown from the saccular walls of the primary septa appears to be the protruding area from the saccular walls of a primary septa and thus has one end attached to the primary septa and the other end suspended open in air space or lumen. In this article, we will present a robust algorithm based on the morphological operations for the segmentation of the secondary septa from the real images of both normal and cancerous lungs.

PREPROCEDURE A: PREPROCESSING

Figure 1(a) shows a typical image of lung tissue in which the bright chambers of the ductal lumens are enclosed by the darker primary walls or septa. The secondary septa appear similar to the primary walls except that they are attached to the primary walls only at one end.

Let a lung septum image of size $N_1 \times N_2$ be represented by a two-dimensional (2D) discrete sequence

Received Mar. 22, 2010; accepted for publication Jul. 19, 2010; published online Dec. 27, 2010.

1062-3701/2011/55(1)/010508/7/\$20.00.

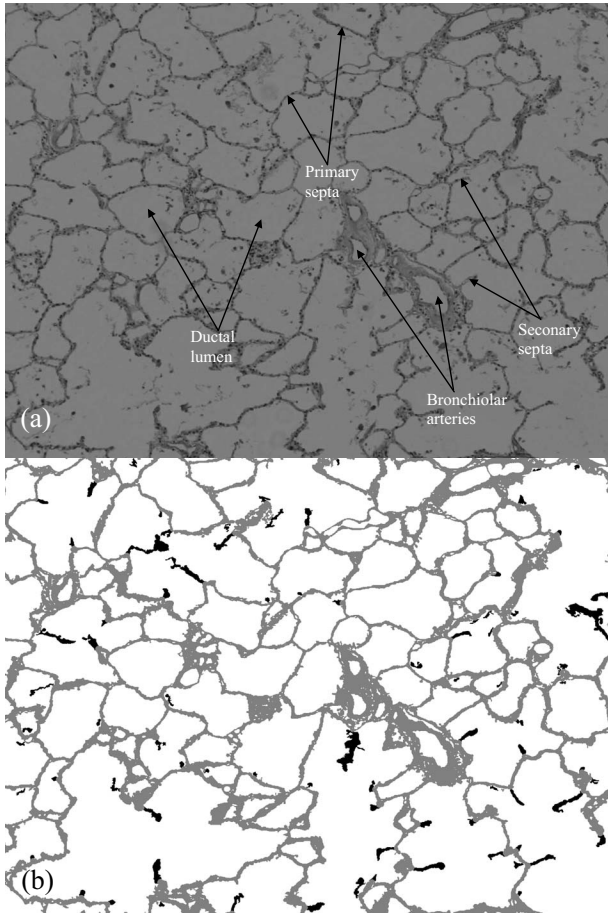


Figure 1. (a) A normal lung image. The secondary septa are those protruding areas from the saccular walls of the primary septa. (b) The dark regions represent the extracted areas of the secondary septa in the lung image. The gray areas include the primary septa and others such as the bronchiolar artery walls.

$$x = \{x(n_1, n_2) | (n_1, n_2) \in D_x\}, \quad (1)$$

in which

$$D_x = \{(n_1, n_2) | 0 \leq n_1 < N_1 \ \& \ 0 \leq n_2 < N_2\}. \quad (2)$$

The septum image such as that in Fig. 1(a) usually has a homogeneous background and much darker walls. A simple global thresholding may be used to exclude the brighter background, such as

$$\Theta = \{(n_1, n_2) | x(n_1, n_2) \leq T; (n_1, n_2) \in D_x\} \quad (3)$$

in which Θ is called the foreground set. Since a location at (n_1, n_2) is always in D_x throughout this paper, Θ can be simplified without ambiguity to

$$\Theta = \{(n_1, n_2) | x(n_1, n_2) \leq T\}. \quad (4)$$

The background set can be written as

$$\bar{\Theta} = \{(n_1, n_2) | x(n_1, n_2) > T\}. \quad (5)$$

Since the proposed algorithm is based on the manipulation of regions, we need a transform to convert a binary image to a set of regions and an inverse transform to convert the set

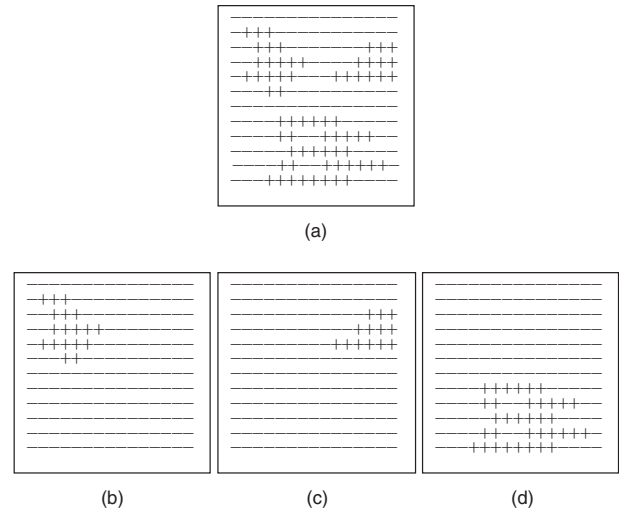


Figure 2. (a) A synthetic set $\bar{\Theta}$ including the points marked by +. The operator $\xi(\bullet)$ transforms $\bar{\Theta}$ in (a) into $\Psi_{\bar{\Theta}}$, a set of three objects of ψ_1 in (b), ψ_2 in (c), and ψ_3 in (d).

of regions back into the binary image. Figure 2 displays an example to show how that transform works. Fig. 2(a) shows a sample binary image in which the “+” sign marks the foreground pixels or member points in $\bar{\Theta}$. Three separate regions are clearly observed in the binary image. The desired transform maps the image to a set of three components as shown in Figs. 2(b)–2(d). We define such a transform as $\xi(\bullet)$ to convert $\bar{\Theta}$ into $\Psi_{\bar{\Theta}}$, a set of regions each of which is composed of all the four-connected elements in the binary image. The transform can be implemented by starting with a new member followed by searching recursively for the four-connected neighboring elements (pixels immediately connected horizontally and vertically) until all elements are exhausted. When applied to the background set $\bar{\Theta}$, we have a set of regions,

$$\Psi_{\bar{\Theta}} = \xi(\bar{\Theta}) = \bigcup_{k=1}^{K_{\bar{\Theta}}} \psi_k, \quad (6)$$

in which $K_{\bar{\Theta}}$ is the total number of separate regions, and each region, ψ_k , is a set of propagated four-connected pixels. Two different regions in $\Psi_{\bar{\Theta}}$, such ψ_k and ψ_l , for $k \neq l$, have no four-connected neighboring elements.

A hole-filling operator $F[\bullet]$ is used to fill the holes inside the region of ψ_k . The holes in the region of ψ_k are sets of the background pixels that cannot be reached by connecting through the background pixels from the edge of the image. Thus, the region $F[\psi_k]$ becomes a solid region without any holes. If the hole-filling operation is applied to a group of separate regions, it applies to the regions individually, such as

$$F[\Psi_{\bar{\Theta}}] = \{F[\psi_k] | 1 \leq k \leq K_{\bar{\Theta}}\}. \quad (7)$$

The set of all the hole points is $\text{XOR}(\bar{\Theta}, \xi^{-1}(F[\Psi_{\bar{\Theta}}]))$, in which $\xi^{-1}(\bullet)$, the inverse operator of $\xi(\bullet)$, converts an object or region back to its components. Organizing the individual

points into the four-connected regions, we have the set

$$\Psi_{\bar{\Theta}}^o = \xi(\text{XOR}(\bar{\Theta}, \xi^{-1}(F[\Psi_{\bar{\Theta}}]))) = \{\psi_{\bar{\Theta},k}^o | 1 \leq k \leq K_{\bar{\Theta}}^o\} \quad (8)$$

in which $K_{\bar{\Theta}}^o$ is the total number of the separate four-connected regions of $\psi_{\bar{\Theta},k}^o$. Let the set

$$\Psi'_{\bar{\Theta}} = \{\xi^{-1}[\psi_{\bar{\Theta},k}^o] | |F[\psi_{\bar{\Theta},k}^o]| < T_1, 1 \leq k \leq K_{\bar{\Theta}}^o\}, \quad (9)$$

where $|\cdot|$ is the size or the total number of elements in the set. The set, $\Psi'_{\bar{\Theta}}$, includes all the elements in the small regions whose sizes are smaller than a given value of T_1 . Since the small regions in $\Psi'_{\bar{\Theta}}$ are likely the loose regions detached from the walls, they are added to the background, to form

$$\Psi_b = \xi(\bar{\Theta} \cup \xi^{-1}(\Psi'_{\bar{\Theta}})), \quad (10)$$

consisting of both the ductal lumens and other small loose specks inside the lumens.

A lumen region should be isolated from any other lumens in Ψ_b . However, there may be occasional thin gaps in both primary and secondary walls creating leaks. If a gap happens in a secondary wall, a part of the secondary wall may be disconnected creating a loose island. The detached island region may still remain outside of Ψ_b since its size is usually larger than a given small threshold of T_1 . If a gap happens in a primary wall, the leak connects the two neighboring lumens. This gap has to be filled in order to avoid the error of misclassifying a piece of primary wall as a part of a secondary wall. The gap is usually very thin such as that shown in Figure 3(a) in which two lumens are connected by the small leak at the end of the dark wall. A morphological open operation with a small 3×3 structure element (SE) can be used to separate the two lumens with only small alterations to the lumen boundaries. Let

$$\Psi_b = \{\psi_{b,k} | 1 \leq k \leq K_b\}, \quad (11)$$

in which the regional set Ψ_b has a total of K_b regions. Let

$$\bar{\Psi}_b(k) = \text{XOR}(\Psi_b, \{\psi_{b,k}\}), \quad (12)$$

the set of all regions except the only one region indexed by k . Applying a morphological open operation with a small SE, size of 3×3 for instance on the single region $\psi_{b,k}$ as shown in Fig. 3(a), we obtain a regional set $\xi\{\text{Open}[\xi^{-1}(\psi_{b,k}), \text{SE}]\}$ that may have more than one region. Discarding the smaller regions, in which the sizes are smaller than T_2 for instance, in $\xi\{\text{Open}[\xi^{-1}(\psi_{b,k}), \text{SE}]\}$ the remaining larger regions are represented by $\bar{\Psi}_{T_2}(k)$. Thus, the complete regional set becomes

$$\bar{\Psi}_{T_2} = \bigcup_{k=1}^{K_b} \bar{\Psi}_{T_2}(k), \quad (13)$$

which is a set of detached regions in which the sizes are larger than T_2 . We can also show



(a)



(b)

Figure 3. Separation of thinly connected lumens. (a) Two lumens are falsely connected because of a thin gap in one of the primary septa, (b) lumens separated with a morphological open operation.

$$\bar{\Psi}_{T_2} = \{\psi_{T_2,k} | 1 \leq k \leq K_{T_2}\}, \quad (14)$$

in which K_{T_2} is the number of regions in $\bar{\Psi}_{T_2}$.

The SE, used in the morphological open operation is a small 3×3 square. Large SE may close wider gaps in the walls. However, larger SE may also introduce larger errors to the walls and other dark points. Thus, the size of SE in the above morphological open operation should be selected as small as possible. If the gap in a primary wall is too large to be closed by a small SE, the broken primary wall may be wrongly recognized as one or two separate pieces of the second walls. The corrections of these broken primary walls will be discussed in the next section.

Procedure A is summarized in the flow chart of Figure 4 in which the input is x , the gray-level image of lung tissue and the output set is

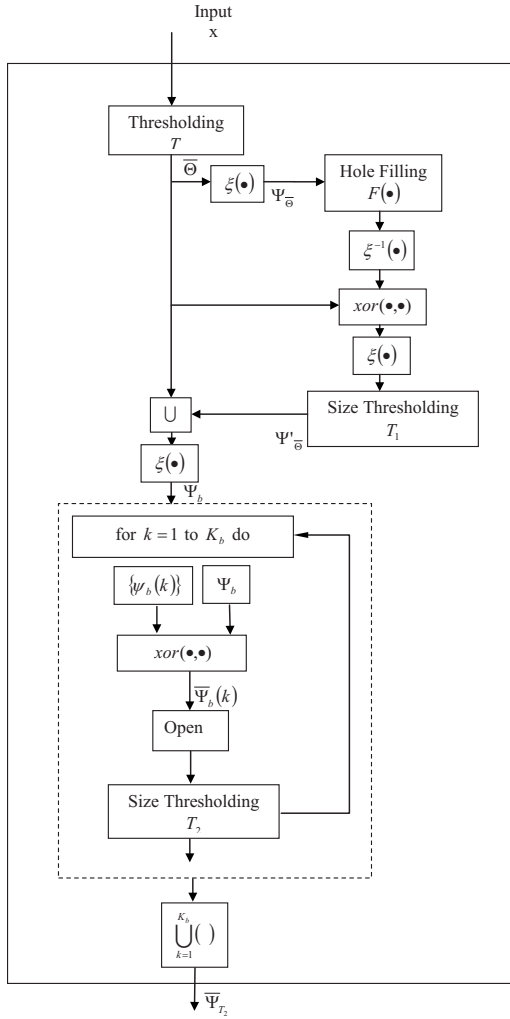


Figure 4. The flow chart of procedure A to create the regional set of $\bar{\Psi}_{T_2}$ from the input image.

$$\bar{\Psi}_{T_2} = \{\psi_{T_2,k} | 1 \leq k \leq K_{T_2}\}, \quad (15)$$

the set of K_{T_2} being separate lumen regions. The block marked by the dashed lines indicates a loop of iterations.

PROCEDURE B: SEGMENTATION OF ONE-ENDED SEPTA

Let $CSE(r)$ be a circular structuring element of radius r defined as

$$CSE(r) = \{(m_1, m_2) | m_1^2 + m_2^2 \leq r^2\}. \quad (16)$$

$CSE(r)$ is the set consisting of elements inside a circular shaped region of radius r , which is centered at the origin.

If the size of k th lumen, $\psi_{T_2,k} \in \bar{\Psi}_{T_2}$, is small enough, for example smaller than $T_3 = 300$, it may not have a significant secondary septum that caves inward. To simplify the computation, those small regions are excluded from consideration. The remaining larger lumens will undergo separately a sequence of dilations and erosions so that such cave-ins can be detected. The procedure is as follows:

```

for k=1 to  $K_{T_2}$  do
{
     $S_k = \phi$ ;
    if  $|\psi_{T_2,k}| \geq T_3$ 
    {
         $b_1 = \text{dilate}(\psi_{T_2,k}, CSE(13))$ ;
         $b_2 = F(b_1)$ ;
         $b_3 = \text{erode}(b_2, CSE(15))$ ;
         $b_4 = \text{XOR}(\psi_{T_2,k}, b_3)$ ;
         $a = b_4 \cap b_3$ ;
         $A = \xi(a)$ , where  $A = \{A_i | i = 1, \dots, I_A\}$ ;
        for i=1 to  $I_A$  do
        {
            if  $(|A_i| \geq T_A)$ 
            {
                 $S_k = S_k \cup A_i$ 
            }
        }
    }
}
    
```

The procedure is a loop consisting of K_{T_2} iterations. To better understand the procedure, we display some intermediate results in Figure 5 to demonstrate the progress of the procedure. At the beginning of the k th iteration, the input is a lumen $\psi_{T_2,k}$ as shown as the white region of Fig. 5(a). Initialized as a null set, S_k accumulates the one-ended septa during the loop of K_{T_2} iterations. If the size, $|\psi_{T_2,k}|$, is too small, the iteration is skipped and the iteration index k is increased by one for the next iteration. The region, $\psi_{T_2,k}$, is dilated with a CSE to obtain a region in which the one-ended septum regions that are slim intrude into $\psi_{T_2,k}$ filled, as shown in Fig. 5(b). We chose the radius of the SE to be 13 so that all of the one-ended septum regions can be changed by the dilation since the thickness of these slim regions is thinner than 25 pixels wide. A hole filling process is then applied to fill in any holes in the dilated region. If the dilated region has no holes such as the one in Fig. 5(b), the hole filling process will have no effect on the region. An erosion process with a lightly larger SE than the previous dilation SE is applied to the dilated region so as to restore the original region, except the one-ended septum regions as shown in Fig. 5(c). The difference between the two regions before and after the erosion yields the regions of the one-ended septum areas and some other smaller and thinner regions as shown in Fig. 5(d). Since the boundary lines of the lumen region appearing in Fig. 5(d) are located outside the lumen, they disappear in the intersection with the lumen region as shown in Fig. 5(e). These smaller regions in Fig. 5(e) are due to the sharp curves along the boundary of the lumen region and thus are excluded. The remaining large regions in S_k are considered as the extracted one-ended septa. The output,

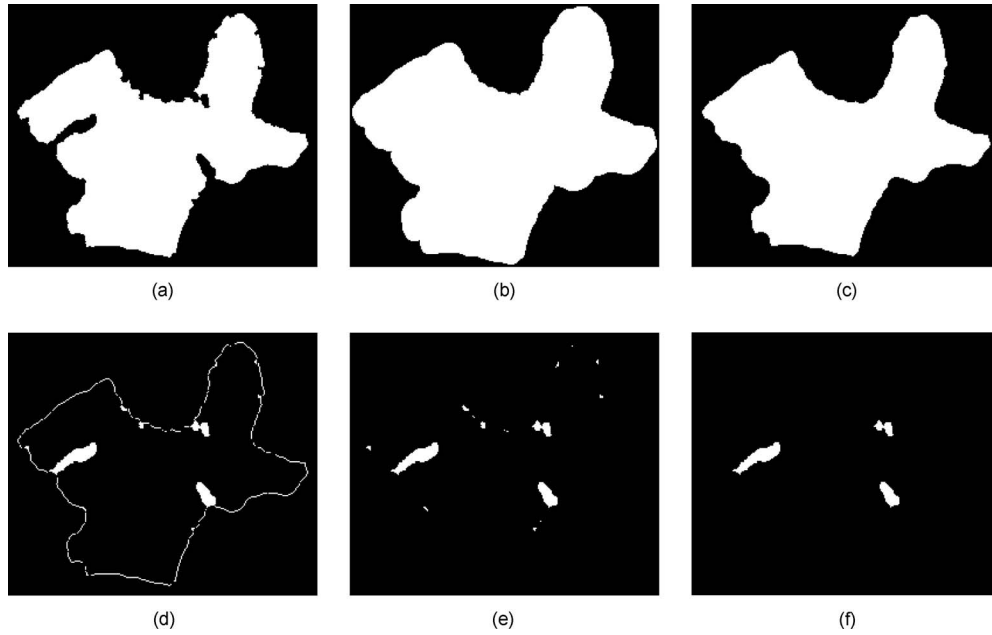


Figure 5. The progress of a single iteration in procedure A of segmenting the one-ended septa. (a) A single lumen in the k th iteration, $\psi_{T_2,k}$; (b) dilation of $\psi_{T_2,k}$ by CSE(13); (c) erosion of the set in (b) by CSE(15); (d) the difference between the sets in (b) and (c); (e) the intersection of the sets in (c) and (d); and (f) the set containing all the regions in (e) larger than the preset size of T_A .

$S = \bigcup_{k=1}^{K_{T_2}} S_k$, is the accumulation of the one-ended septa in all of the iterations.

RESTORATION OF THE BROKEN PRIMARY SEPTA

In practice, a primary septum may occasionally appear broken. Thus, the broken primary septum may be considered as one or two secondary septa because it may appear as one or two single-ended extensions. If a leak or gap in a primary septum is very thin, for example, one or two pixels wide, a morphological open operation of small structuring elements in the lumen regions (equivalent to a morphological close operation to the septum regions) may close it with insignificant errors at the regional boundaries. However, when the gap is wider it will be difficult to close the gap since applying an operation with a larger structuring element may also introduce a higher level of distortion.

To deal with the primary septa having wide gaps, we examined the difference between the broken primary septa and the real secondary septa. A broken primary septum appears as two separate regions that are close in distance while a secondary septum is one isolated region that is relatively far from the other secondary septa. Our approach in separating the secondary septa from the broken primary septa in the one-ended septum pool, S , is to try and bridge the gaps between any two single-ended septa.

The procedure is summarized in the chart of Figure 6. The inputs are the two sets, $\bar{\Psi}_{T_2}$ and S , the two outputs from the procedures A and B. The set $\bar{\Psi}_{T_2}$ contains lumen regions while S contains the one-ended septum regions. The union $\bar{\Psi}_{T_2} \cup S$ includes both the lumen and one-ended septum regions and excludes the other septum regions connected on both sides. Thus, the negation $P = \sim(\bar{\Psi}_{T_2} \cup S)$ contains the

primary septum regions. We apply a morphological dilation with a round SE of radius r_p to P and obtain the output $DiP = \text{dilate}(P, SE(r_p))$. $\bar{\Psi}_{T_2}$ has a total of K_{T_2} lumen regions.

The one-ended septa next to $\psi_{T_2,k}$, the k th lumen in $\bar{\Psi}_{T_2}$, are in S_k . If the regions in S_k are morphologically dilated by a round SE of radius r_p such as $DiS_k = \text{dilate}(S_k, SE(r_p))$, these dilated regions may have portions overlapping with those in DiP . The binary image of the overlapped areas is

$$g_k = \xi^{-1}(DiP) \cap \xi^{-1}(DiS_k). \quad (17)$$

The image g_k may have several small isolated regions. Let the set G_k contain all of the regions in the binary image of g_k . Since each region in G_k is adjacent to two regions in $P \cup S_k$, those adjacent to two regions already touching should be removed. The remaining regions $G_k^- \subset G_k$ are accumulated and finally added to the set S so that the gaps are filled. Let $G^+ = \bigcup_{k=1}^{K_{T_2}} G_k^-$. The set G^+ contains all of the small regions that bridge the gaps between septum regions. The set $P \cup S \cup G^+$ includes both primary and secondary septa and the bridging regions. Its complement includes all of the lumen regions again processed by procedure B so that the new single-ended septa are obtained. Since the broken primary septa are repaired after filling the gaps, the single-ended septa obtained this time are considered as the secondary septa.

RESULTS

Fig. 1(a) shows the original image of a normal lung consisting of bronchiolar arteries surrounded by thick walls, ductal lumens of the air spaces, primary septa or walls that enclose the air sacs, and the secondary septa outgrowing from the saccular walls of the primary septa as indicated by the over-

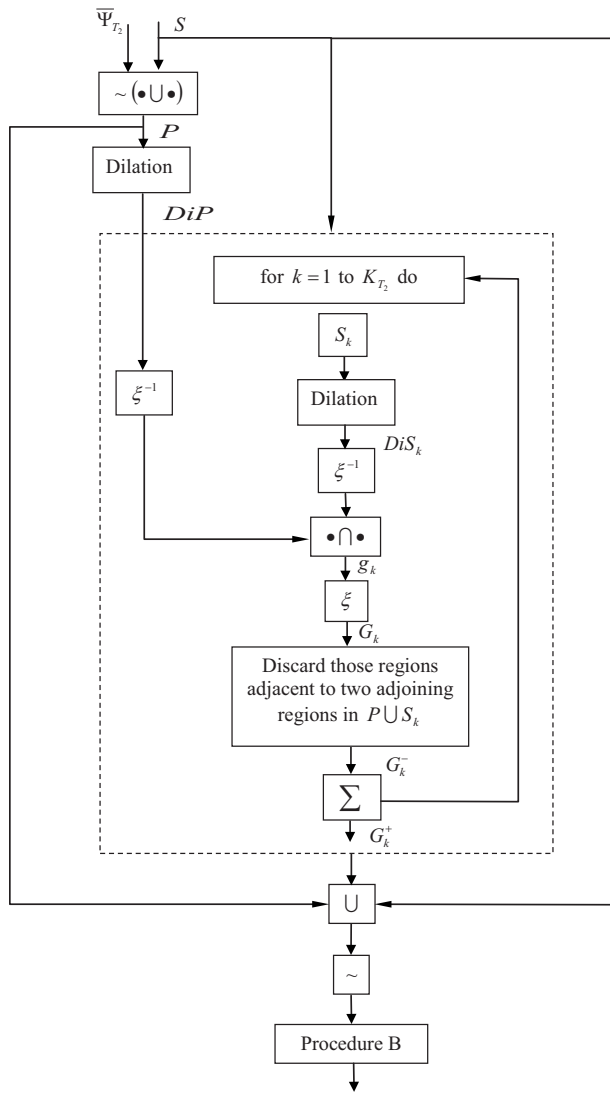


Figure 6. The flow chart of restoring the broken primary septa.

lay arrows. Since the secondary septa are grown out of the primary walls, they appear to be the protruding areas from the saccular walls of the primary septa and thus have one end contacted to the primary septa with the other end suspended in air. The image is size 1280×960 . Fig. 1(b) shows the segmentation of the secondary septa from the image in (a). The dark regions represent the extracted areas of the secondary septa in the lung image while the gray areas include the primary septa and other areas such as the bronchiolar artery walls. The visual comparison between the dark regions in the segmentation and the secondary septa of the original image demonstrates that the segmented regions match well to the secondary septum regions.

Figure 7 displays additional segmentation results of the secondary septa from both normal and cancerous lungs. Fig. 7(a) shows an image of normal lung. Fig. 7(a') is its corresponding segmentation for the secondary septa. Figs. 7(b) and 7(c) show two images of cancerous lungs while Figs. 7(b') and 7(c') show the segmentations of their secondary septa, respectively. Comparing the original images on the left column in Fig. 7 with their respective segmentation of the secondary septa as the dark intensity in the right column, we conclude that the extracted regions match very well to the real secondary septum regions. Thus, the proposed algorithm performs very well and produces accurate segmentations for the secondary septa in lungs.

DISCUSSION AND CONCLUSIONS

Quantization of structural components of the lung has always been one of the prime objectives of biological morphometry.^{17,18} To evaluate the features, a segmentation of the lung images is a prerequisite in order to separate the desired regions from the remainder so that all of the quantization are performed only on the desired regions. The secondary septa in lungs are outgrown from the primary walls and thus are differentiated from the primary walls in the sense that each has only one end attached to a primary wall

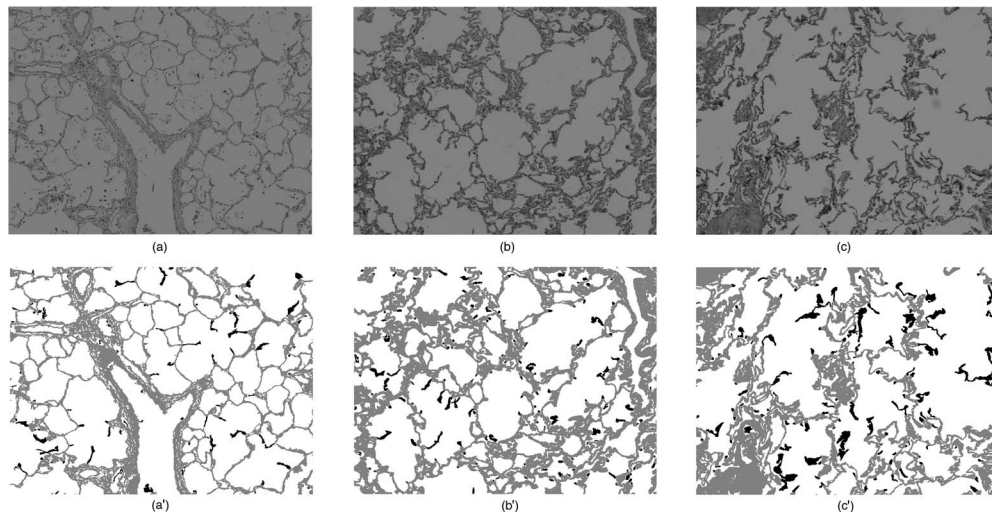


Figure 7. (a) An image of normal lung; (a') segmented secondary septa indicated by the dark regions; [(b) and (c)] two images of cancerous lungs; [(b') and (c')] extracted secondary septa from images in (b) and (c), respectively.

and the other end is loose in the air. In real application, leaks that can happen to both primary and secondary walls may make the segmentation task difficult. To have a robust segmentation algorithm, we have to fill those possible leaks while also retaining all the other parts as similar as possible. In the current manuscript, we use two gap-filling steps to fill the leaks. The first gap-filling step is to use a morphological close operation with a small SE to fill the thinnest leaks as shown in Fig. 3. Lumen regions are then extracted and isolated from each other. Adjoining each lumen are the primary septa and also possibly the secondary septa. A procedure is designed to extract the single-ended septum regions (only one end is in touch with the outside of the lumen) adjacent to the same lumen. Among the recognized single-ended septum regions, the broken primary septa and the real secondary septa are differentiated by calculating their distances. The second gap-filling step is then to fill up the wider gaps by adding small regions between the two ends of the broken primary septum regions. The real secondary septa are then identified by again extracting the single-ended septum regions again from the image in which the leaks in the septum regions are repaired.

The results of both normal and cancerous lungs are presented. The results show the accuracy of the segmentations of the secondary septa based on the visual comparisons between the real secondary septa and the segmented ones. The algorithm is robust since the imperfect septum regions with possible leaks in the real images are repaired before the single-ended septum regions are segmented.

REFERENCES

- ¹M. Ochs, P. H. Burri, J. Gil, and E. R. Weibel, "Ultrastructure and morphometry of the human lung", in *General Thoracic Surgery*, 7th ed., edited by T. W. Shields et al. (Williams and Wilkins, Philadelphia, 2009), Vol. 1, pp. 39–59.
- ²T. B. Zeltner and P. H. Burri, "The postnatal development and growth of the human lung. II. Morphology", *Respir. Physiol.* **67**, 269–282 (1987).
- ³R. Harding, K. Snibson, M. O'Reilly, and G. Maritz, in "Early environmental influences on lung development: Implications for lung function and respiratory health throughout life", in *Early Life Origins of Human Health and Disease*, edited by J. P. Newnham and M. G. Ross (Karger, Basel, 2009), pp. 78–88.
- ⁴M. R. Chinoy, S. A. Miller, R. L. Myers, R. E. Cilley, and P. W. Dillon, "Persistent vascular defects in lung allografts attributed to defective endogenous endothelial progenitors", *J. Surg. Res.* **124**, 14–22 (2005).
- ⁵S. A. Tschanz and P. H. Burri, "A new approach to detect structural differences in lung parenchyma using digital image analysis", *Exp. Lung Res.* **28**, 457–471 (2002).
- ⁶D. McCurrin, S. Seidner, L.-Y. Chang, N. Waleh, M. Ikegami, J. Petershack, B. Yoder, L. Giavedoni, K. H. Albertine, M. J. Dahl, Z.-M. Wang, and R. I. Clyman, "Ibuprofen-induced patent ductus arteriosus closure: Physiologic, histologic, and biochemical effects on the premature lung", *Pediatrics* **121**, 945–956 (2008).
- ⁷I. Hosgör, A. Yarat, N. Tüzüner, F. Alkan, N. Emekli, and S. Ahmad, "Biochemical and morphological alterations in lungs induced by experimental inhibition of fibrinolytic activity", *Mol. Cell. Biochem.* **241**, 9–19 (2002).
- ⁸O. Boucherat, A. Benachi, A.-M. Barlier-Mur, M.-L. Franco-Montoya, J. Martinovic, B. Thebaud, B. Chailley-Heu, and J. R. Bourbon, "Decreased lung fibroblast growth factor 18 and elastin in human congenital diaphragmatic hernia and animal models", *Am. J. Respir. Crit. Care Med.* **175**, 1066–1077 (2007).
- ⁹J. J. Foster, K. L. Goss, C. L. S. George, P. J. Bangsund, and J. M. Snyder, "Galectin-1 in secondary alveolar septae of neonatal mouse lung", *Am. J. Physiol. Lung Cell. Mol. Physiol.* **291**, L1142–L1149 (2006).
- ¹⁰S. Cativa Tolosa, S. Blacher, A. Denis, A. Marajofsky, J.-P. Pirard, and C. J. Gommès, "Two methods of random seed generation to avoid over-segmentation with stochastic watershed: Application to nuclear fuel micrographs", *J. Microsc.* **236**, 79–86 (2009).
- ¹¹S. Huh, D. Lee, and R. F. Murp, "Efficient framework for automated classification of subcellular patterns in budding yeast", *Cytometry, Part A* **75A**, 934–940 (2009).
- ¹²H.-S. Wu, M. I. Fiel, T. D. Schiano, and J. Gil, "Image segmentation of liver fibrosis", *J. Microsc.* **231**, 70–80 (2008).
- ¹³M.-R. Jeong, B. C. Ko, and J.-Y. Nam, "Overlapping nuclei segmentation based on Bayesian networks and stepwise merging strategy", *J. Microsc.* **235**, 188–198 (2009).
- ¹⁴H.-S. Wu, R. Xu, N. Harpaz, D. Burstein, and J. Gil, "Segmentation of intestinal gland images with iterative region growing", *J. Microsc.* **220**, 190–204 (2005).
- ¹⁵H.-S. Wu, J. Murray, and S. Morgello, "Segmentation of brain immunohistochemistry images using clustering of linear centroids and regional shapes", *J. Imaging Sci. Technol.* **52**, 040502 (2008).
- ¹⁶H.-S. Wu, M. Bitar, D. Burstein, M. Ramer, and J. Gil, "An envelope mapping algorithm and its applications in enhancement and segmentation of pancreatic cell images", *J. Imaging Sci. Technol.* **53**, 030501 (2009).
- ¹⁷E. R. Weibel, C. C. W. Hsia, and M. Ochs, "How much is there really? Why Stereology is essential in lung morphometry", *J. Appl. Physiol.* **102**, 459–467 (2007).
- ¹⁸L. Knudsen, E. R. Weibel, H. J. G. Gundersen, F. V. Weinstein, and M. Ochs, "Assessment of airspace size characteristics by intercept (chord) measurement: An accurate and efficient stereological approach", *J. Appl. Physiol.* (2009).